Arts & Sciences Articles

Arts and Sciences

6-22-2018

Topological Changes of Wave Functions Associated with Hamiltonian Monodromy

C. Chen

John B. Delos
William & Mary, jbdelo@wm.edu

Topological changes of wave functions associated with Hamiltonian monodromy

C. Chen and J. B. Delos[*]

Physics Department, William & Mary, Williamsburg, Virginia 23185, USA

Almost everything that happens in classical mechanics also shows up in quantum mechanics when we know where to look for it. A phenomenon in classical mechanics involves topological changes in action-angle loops as a result of passage around a "monodromy circuit." This phenomenon is known by the short name "Hamiltonian monodromy" (or, more ponderously, "nontrivial monodromy of action and angle variables in integrable Hamiltonian systems"). In this paper, we show a corresponding change in quantum wave functions: These wave functions change their topological structure in the same way that the corresponding classical action-angle loops change.

I. INTRODUCTION

"Monodromy" means "once around a closed path"; a system exhibits "nontrivial monodromy" if when we go around a closed path, the system does not come back to its original state. The simplest example is the square root function in the complex plane—upon one circuit around the origin, the square root changes sign. "Hamiltonian monodromy" refers specifically to multivaluedness of action-angle variables. This phenomenon occurs in a variety of classical and quantum systems: any cylindrically symmetric system with a quadratic barrier, the spherical pendulum, dipolar molecules in fields, the hydrogen atom in crossed fields, nearly linear molecules, elliptical billiards, and atoms in traps [1–18].

As a representative case, let us consider particles moving in two dimensions in a circularly symmetric "champagne bottle" or "Mexican hat" potential energy:

$$H(\boldsymbol{q},\boldsymbol{p}) = \frac{p_x^2 + p_y^2}{2\mu} + V(\rho),$$

$$V(\rho) = -\frac{3}{2}\rho^2 + \frac{1}{60}\rho^4,$$

$$\rho = (x^2 + y^2)^{1/2},$$

$$\varphi = \tan^{-1}(y/x). \tag{1}$$

There are two conserved quantities, angular momentum $L(\boldsymbol{q},\boldsymbol{p}) = x\,p_y - y\,p_x$ with conserved value l and energy (the Hamiltonian function itself), having conserved value E. A "level set" is the set of points $(\mathbf{q},\mathbf{p})$ in phase space corresponding to fixed values of angular momentum and energy. For the Mexican hat system, by general theorems in classical mechanics [19], every level set except one is a torus, and the shape in phase space of these tori, and the motion on them as well, can be described by action-angle variables. The values of action variables specify the torus on which the motion occurs, and the values of angle variables specify the position on each torus. As each angle variable is varied between 0 and 2π

(holding the other fixed), the phase-space point traces out a fundamental loop on the torus.

The exceptional level set is the one having $l = 0$ and $E = 0$. That set (like all the others) is cylindrically symmetric, but it is a "pinched torus," like the ∞ symbol rotated about a vertical axis in the plane of the paper. This seeming violation of general theorems occurs because the gradients of $L(\boldsymbol{q},\boldsymbol{p})$ and $H(\boldsymbol{q},\boldsymbol{p})$ both vanish at $(\boldsymbol{q} = \boldsymbol{0}, \boldsymbol{p} = \boldsymbol{0})$; accordingly the origin in phase space $(\boldsymbol{q} = \boldsymbol{0}, \boldsymbol{p} = \boldsymbol{0})$ is called a "singular point." Connecting with the language of quantum mechanics, we call the two-dimensional space of values of conserved quantities (l, E) "spectrum space" (also called angular momentum, energy space). The origin in phase space $(\boldsymbol{q} = \boldsymbol{0}, \boldsymbol{p} = \boldsymbol{0})$ corresponds to the origin in spectrum space, $(l = 0, E = 0)$, and this point is called a "singular value," which we call the "monodromy center."

Action-angle variables are not defined on this level set and the remaining set of nonsingular values in spectrum space is not simply connected. A consequence is that action-angle variables can, and in fact do, become multivalued functions of (l, E). When we examine the changes of action and angle loops as we travel around any closed circuit surrounding the monodromy center, the initial and final tori are the same. However, the loop traced out by one of the angle variables smoothly changes into a different fundamental loop on the torus (Fig. 1). This is called a "static" manifestation of monodromy.

In Refs. [20,21] it was pointed out that this static manifestation of monodromy must have dynamical consequences: If a collection of noninteracting particles is given initial conditions corresponding to an initial angle loop on a torus, and those particles are driven continuously by an ideal Hamiltonian flow around a monodromy circuit, then the loop of particles undergoes the same topological change that is seen in the angle loop. In Ref. [22], simulations showed that this phenomenon can be observed under a relatively simple time-dependent Hamilton when the appropriate torque is applied. Furthermore, the topological change also occurs under less-than-ideal conditions, with particles having a distribution of energies and angular momenta.

The question we address in this paper is whether we can construct quantum wave functions that have the same topological

─────────
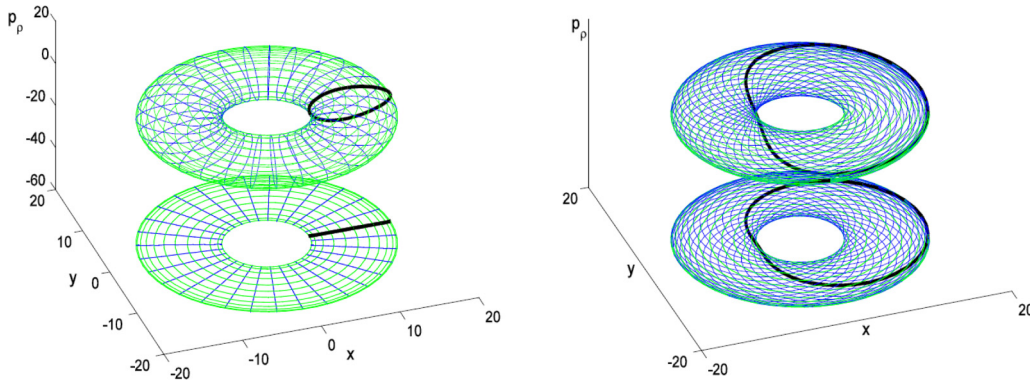[*]Corresponding author: jbdelo@wm.edu

FIG. 1. In each figure is a torus in phase space specified by $(l = 0, E = E_0 < 0)$ and its projection onto the x-y plane. The two tori are exactly the same two-dimensional manifold in four-dimensional phase space, but with different coordinate systems on them, defined by angle variables (ϕ_1, ϕ_2). The bold black (online) loop is a selected action-angle loop, defined by $\phi_1 = $ const., $0 < \phi_2 < 2\pi$. On the left it is a poloidal loop, and other poloidal loops are shown at different fixed values of ϕ_1 (blue online). Toroidal loops (green online) have $\phi_2 = $ const., $0 < \phi_1 < 2\pi$. Initially, the bold black (online) action-angle loop stays on one side of the central forbidden region. When (l, E) change smoothly on a monodromy circuit, the corresponding torus also changes smoothly, and so does the action-angle loop. After traversing a monodromy circuit, when (l, E) return to their initial values $(l = 0, E = E_0 < 0)$, the torus returns to the original torus but the action-angle loop has changed into a topologically different loop, shown in the figure on the right. These loops are used for calculating action variables, so the value of the corresponding action can also change on a monodromy circuit.

change that is seen in the action-angle loops. The answer is yes. In this paper, we will show (1) a static quantum manifestation of monodromy—we define a superposition of eigenfunctions of H which has the appearance of an initial action-angle loop, confined to one side of a classically forbidden region; when we carry this superposition around a monodromy circuit in spectrum space, the wave function changes its structure to a loop that surrounds the classically forbidden region. We show also (2) an analogous "ideal" dynamical quantum manifestation of monodromy: We define a continuous time-dependent unitary transformation, which drives the expectation values of angular momentum and energy around a monodromy circuit, and which causes the wave function to make the same topological change. Finally we show (3) a realizable manifestation—this topological change can be implemented by a time-dependent Hamiltonian with an appropriate radiation field.

One result is shown in Fig. 2. Before being carried around the monodromy circuit, the wave function is localized on one side of the origin. Afterwards it surrounds the origin. (Spreading of a wave packet cannot produce the change shown here. In our case, spreading occurs on a longer time scale, and produces a different density.)

Everything in this Introduction will be explained in detail in the following sections.

II. RELATIONSHIP TO OTHER WORK

This work is connected with the theory of torus quantization (the modern version of the old quantum theory) which has been used to study an immense variety of systems, including simple nonlinear oscillators, molecular vibrations and rotations, excited states of hydrogen in electric and magnetic fields, doubly excited states of helium, spin-orbit coupling, and excited states of nuclei [23–31]. For the Mexican hat system, Duistermaat, following a suggestion by Cushman,

constructed action-angle variables, and showed that smoothly defined action-angle variables cannot be single valued. Subsequently, Cushman and Duistermaat described the quantum implications of multivalued action variables: The lattice of allowed semiclassical eigenvalues, defined by quantization of these multivalued action variables, has a defect [32–34]. In Fig. 3, we see that a unit cell carried around a monodromy circuit does not return to itself.

As mentioned earlier, many classical and quantum systems display Hamiltonian monodromy and its associated spectral defects. This seemingly abstract geometry in phase space leads to interesting dynamical consequences: In a system like the Mexican hat, if the system is subjected to appropriate perturbations, a loop of particles can evolve smoothly in time into a topologically different loop [20–22].

Monodromy is the simplest and most accessible example of a class of recently uncovered phenomena (bidromy and fractional monodromy), and it also shows up in attractors in field theory [35–39]. It was discovered because of new ways of thinking about classical Hamiltonian systems (the global perspective—how tori fit together in phase space) [40,41]. As stated earlier, the topological change in wave functions shown in Fig. 2 is a quantum analog of the topological change in action-angle loops.

Finally, topological quantum states receive much attention because they are connected with the integer or fractional quantum Hall effect, because certain atom transport schemes use topological methods, and because of speculations that they can be used to implement schemes for topological quantum computing [42–54]. Indeed, 57 presentations at the 2017 DAMOP meeting and 958 presentations at the 2017 APS March meeting dealt with topological changes in quantum and classical states, mainly in many-body systems. In Fig. 2, we have shown by computation that quantum states of very simple two-dimensional systems also can display interesting topological changes.
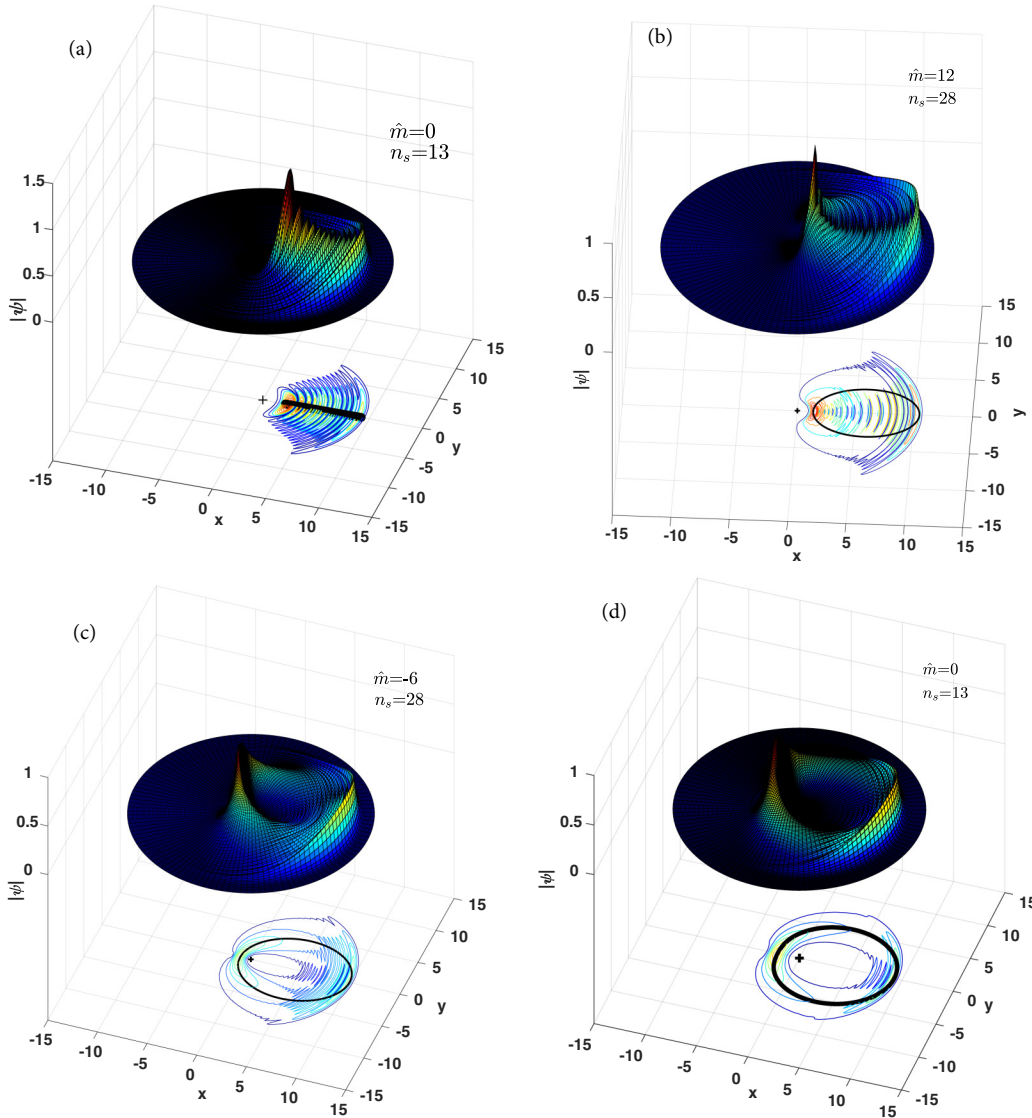
FIG. 2. Monodromy of wave functions. Initially we make a superposition with expectation value of angular momentum $\langle l \rangle = 0$, and expectation value of energy $\langle E \rangle = E_{m=0,n_r=13}$, shown in (a). This superposition is localized on one side of the classically forbidden region. The contour plot corresponds with the black angle loop specified by $(\langle l \rangle = 0, \langle E \rangle = E_{m=0,n_r=13})$. After $(\langle l \rangle, \langle E \rangle)$ are carried smoothly around the monodromy circuit and return to their original values $(\langle l \rangle = 0, \langle E \rangle = E_{m=0,n_r=13})$, the wave function smoothly changes into a topologically different wave function, corresponding with the topologically changed angle loop (d). (b,c) are superpositions whose expectation values of angular momentum and energy correspond, respectively, to the (l, E) point on the upper right corner of the monodromy circuit in Fig. 3 $[(\langle l \rangle = 12, \langle E \rangle = E_{m=12,n_r=28})]$ and the point on the upper left corner of that monodromy circuit $[(\langle l \rangle = -6, \langle E \rangle = E_{m=-6,n_r=22})]$. The quantum numbers n_r and n_s are defined later in Sec. III.

III. SMOOTH ACTION VARIABLES AND THEIR ASSOCIATED QUANTUM NUMBERS

Action variables are defined as integrals around fundamental loops on the tori:

$$I = \oint_C \mathbf{p} \cdot d\mathbf{q}/2\pi. \tag{2}$$

C refers to one of the fundamental loops of the torus. In a naïve application of this formula to circularly symmetric systems, one might presume that the two fundamental loops are radial and angular:

$$I_{\text{ang}} = \oint_{C_1} \mathbf{p} \cdot d\mathbf{q}/2\pi = p_\varphi = l, \tag{3}$$

$$I_{\text{rad}} = \oint_{C_2} \mathbf{p} \cdot d\mathbf{q}/2\pi = 2\int_{\rho_{\min}}^{\rho_{\max}} p_\rho d\rho/2\pi. \tag{4}$$

C_1 is a loop at fixed ρ and C_2 is a loop at fixed φ [Fig. 1(a)]. I_{ang} is a good action variable, but I_{rad} is not: One can show that $(\frac{\partial I_{\text{rad}}}{\partial l})_E$ is discontinuous at $l = 0$ and $E > 0$. We need action variables that are differentiable functions. Many earlier references have shown that this action can only be a smooth
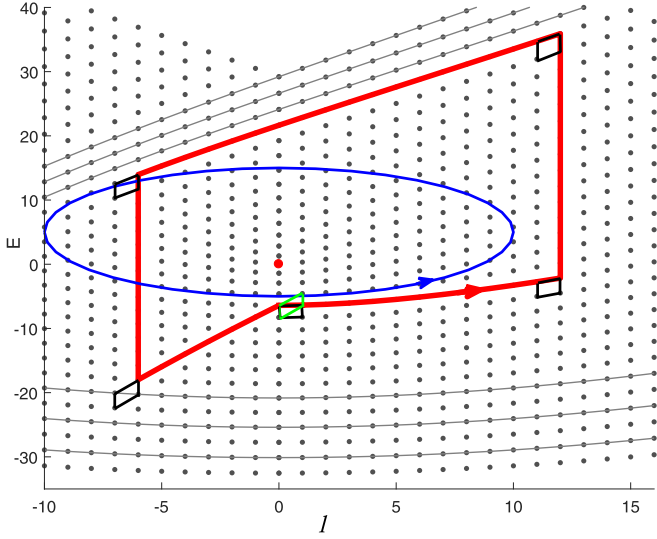
FIG. 3. Monodromy circuits. Coordinates of spectrum space for this system are angular momentum and energy. The gray dots represent quantized eigenvalues (m, E_{m,n_r}) for the Mexican hat system defined in Eq. (1). The gray (online) curves link states of the same "quantized smooth action variable." The origin, marked by a large red (online) dot, is a singular value, also called a monodromy center. Any closed circuit [such as the elliptical blue (online) curve] around this point is a classical monodromy circuit. The bold red (online) circuit is the quantum monodromy circuit that we often follow. The defect in the spectrum is shown by transport of a unit cell around the monodromy circuit, where it returns to a different unit cell (green online, light gray in print).

function of (l, E) if it is multivalued, with a branch point at the monodromy center ($l = 0, E = 0$).

There are many ways to choose the second action variable so that it is smooth (see Fig. 4 of Ref. [21]). We choose the following. Define the effective Hamiltonian:

$$\mathcal{H}(\boldsymbol{q},\boldsymbol{p};l,E) = H(\boldsymbol{q},\boldsymbol{p}) - \Omega(l,E)L(\boldsymbol{q},\boldsymbol{p}). \quad (5)$$

Here $\Omega(l,E) = \Theta(l,E)/T(l,E)$ is the angular velocity averaged over a cycle of radial motion—$T(l,E)$ is the radial period (time for return to the original value of ρ with the original value of p_ρ), and $\Theta(l,E)$ is the azimuthal angle subtended in one radial period. Both quantities are obtained from trajectories of $H(\boldsymbol{q},\boldsymbol{p})$, and they must be defined so that they are differentiable functions of (l,E) everywhere except at the monodromy center. It follows that $\Theta(l,E)$ must be a multivalued function. We take the convention that we begin with $(l = 0, E < 0)$, where $\Theta(l,E) = 0$. Upon passage around a counterclockwise monodromy circuit, $\Theta(l,E)$ increases by 2π. (See Fig. 9 of Ref [21].) Trajectories under $\mathcal{H}(\boldsymbol{q},\boldsymbol{p};l,E)$ are obtained by treating (l,E) as fixed parameters, and by obtaining Hamiltonian equations of motion from the $(\boldsymbol{q},\boldsymbol{p})$ dependence of $\mathcal{H}$. These trajectories have the form of trajectories under $H(\boldsymbol{q},\boldsymbol{p})$ as seen in a frame of reference rotating counterclockwise with angular velocity $\Omega(l,E)$. Hence in one radial cycle, every orbit closes. Any trajectory of $\mathcal{H}(\boldsymbol{q},\boldsymbol{p};l,E)$ is an action-angle loop. The canonical angle variable associated with this loop increases linearly with time from zero to 2π as the trajectory under $\mathcal{H}(\boldsymbol{q},\boldsymbol{p};l,E)$ goes around the loop, and the
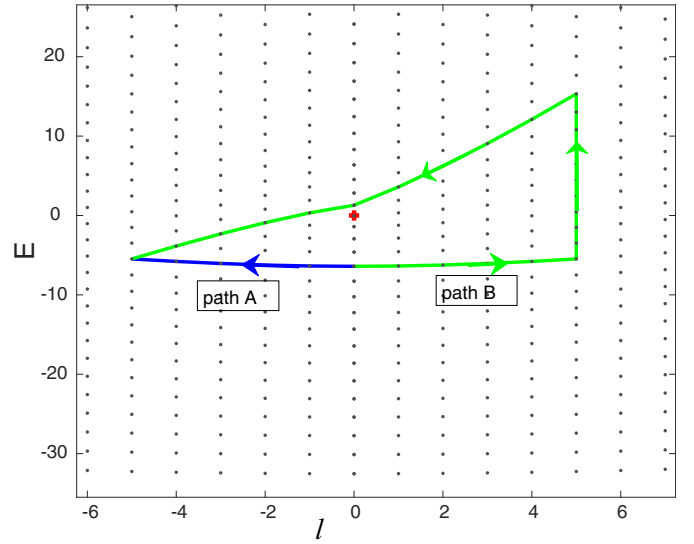

FIG. 4. Path dependence of phase. The phase $ph(m = -5, n_r = 13)$ can be defined either by path A (blue online, dark gray in print) or path B (green online, light gray in print). The starting point of the two paths is $m = 0$, $n_r = 13$, with $ph(m = 0, n_r = 13) = 1$. If the phase $ph(m = -5, n_r = 13)$ is defined along path A, according to the rule in Eq. (17), $ph_A(m = -5, n_r = 13) = 1$. If the phase $ph(m = -5, n_r = 13)$ is defined along path B, according to the rule in Eq. (16), since the path crosses the $m = 0$ axis with $E > 0$, $ph_B(m = -5, n_r = 13) = -1$.

action variable is given by the integral

$$I_s = \int_0^{T(l,E)} \boldsymbol{p}(\tau)\frac{d\boldsymbol{q}(\tau)}{d\tau}d\tau/2\pi \quad (6)$$

around the loop. We call $I_s(l,E)$ the "smooth action variable"; it is a multivalued differentiable function of (l,E) everywhere except at the monodromy center.

In the Supplemental Material for this paper [55], we show pictures of the two families of action-angle loops for this system. These action-angle loops define a coordinate system on each torus. In our images, such as Fig. 1, we represent the tori using (x, y, p_ρ) as coordinates. Initially [Fig. 1(a)], with $l = 0$, $E < 0$, and $\Theta(l,E) = 0$, the I_s loop is poloidal. The relationship between those coordinates on one torus and on another constitutes a *connection* between coordinates on the different tori. As we change (l,E), moving from one torus to another, these action-angle loops obtained from the effective Hamiltonian, and the associated coordinate systems on the tori, change gradually and smoothly, provided that we make $\Theta(l,E)$ change smoothly. A "monodromy circuit" is any continuous closed path in spectrum space surrounding the monodromy center (Fig. 3). If we carry the system around such a path, when the system returns to its original (l,E), the topological structure of the $\mathcal{H}$ family of loops is different (Fig. 1). The poloidal loop changes to a combination of toroidal and poloidal loops. This happens because $\Theta(l,E)$ changes from zero to 2π on traversing the monodromy circuit. When we calculate I_s using (6), we must follow this angle loop with its topological change.

The multivalued nature of I_s follows from the change of structure of the loop. We begin by using Eq. (4) for $l > 0$; then

if we cross to $l < 0$ below the monodromy center ($E < 0$), the simple radial integral, Eq. (4), gives an analytic continuation to negative l, and

$$I_s(-|l|,E) = I_s(|l|,E) \quad (E < 0). \tag{7}$$

However, if we cross to $l < 0$ above the monodromy center ($E > 0$), this smooth action I_s is given by

$$I_s(-|l|,E) = I_s(|l|,E) - l \quad (E > 0). \tag{8}$$

With continuing counterclockwise circuits about the monodromy center, every time we cross $l = 0$ with $E > 0$, l is subtracted, giving a multivalued but smooth action.

Quantum eigenenergies can be calculated with good accuracy using a semiclassical approximation, by quantization of the action variables:

$$I_{\mathrm{ang}} = l = m\hbar, \tag{9}$$

$$I_{\mathrm{rad}}\big(m,E_{m,n_r}\big) \simeq \big(n_r - \tfrac{1}{2}\big)\hbar. \tag{10}$$

Alternatively, we may label quantum states using the smooth action variable,

$$I_s\big(m,E_{m,n_s}\big) \simeq \big(n_s - \tfrac{1}{2}\big)\hbar. \tag{11}$$

$m = \cdots - 2, -1, 0, 1, 2, \cdots$ is the angular momentum quantum number. $n_r = 1, 2, \cdots$ is the familiar radial quantum number. It is uniquely defined for each quantum state, but corresponds to an unsmooth action variable. In contrast, n_s is a quantum number associated with the smooth but multivalued action, I_s, and it is therefore also multivalued.

Equivalently, any quantum state has definite values of m and n_r, but it has many possible assignments of n_s. If we begin with $n_s = n_r$ with $m > 0$, then upon crossing to $l < 0$ with $E > 0$, n_s becomes $n_r - m$. (This may seem like a reason to avoid its use, but there are dynamical processes in which the classical system follows the smooth action variable I_s, and the quantum system follows the corresponding quantum number n_s.)

Figure 3 shows the spectrum of quantum energy levels. On this scale there is no visible difference between semiclassical and exact quantum eigenvalues. Contours of smooth action are also shown.

IV. CONSTRUCTION OF WAVE FUNCTIONS WITH TOPOLOGICAL CHANGES

In the Introduction we have shown a quantum manifestation of monodromy in superpositions of eigenfunctions: A topological change in the structure of the superposition. Here we define the superpositions which give that topological change. The motivations for the methods presented in this section come from classical and semiclassical mechanics, and from study of simpler systems. Those are discussed in Sec. V.

A. Eigenfunctions and eigenvalues of the Mexican hat system

With the quantum Hamiltonian from Eq. (1),

$$\left[-\frac{\hbar^2}{2\mu}\nabla^2 + V(\rho,\varphi) \right]\chi_{m,n_r}(\rho,\varphi) = E_{m,n_r}\chi_{m,n_r}(\rho,\varphi), \tag{12}$$

we define *for $m \geqslant 0$ only*,

$$\chi_{m,n_r}(\rho,\varphi) = N_{m,n_r}\exp(im\varphi)R_{n_r}^m(\rho), \tag{13}$$

with the following conventions. For each $m \geqslant 0$, n_r labels the eigenvalues and eigenfunctions in order of energy, starting at $n_r = 1$. Like Bessel functions, $R_{n_r}^m(\rho)$ approaches ρ^m as ρ approaches the origin; i.e., $R_{n_r}^m(\rho)$ is positive near the origin. As ρ increases, $R_n^m(\rho)$ oscillates, with $n_r - 1$ zeros, and then decays exponentially at large ρ. N_{m,n_r} is a real and positive normalizing constant. These eigenfunctions for $m \geqslant 0$ were computed by expansion in a Bessel function basis.

The spectrum of energy levels can be extended to $m < 0$ by the rule $E_{-|m|,n_r} = E_{|m|,n_r}$. In this way we are again labeling states with fixed $m < 0$ in order of their energies, again starting with $n_r = 1$ for each m. For $|m|$ small, the eigenvalues E_{m,n_r} for fixed n_r lie close to a parabola when $E_{m,n_r} < 0$, but close to a line with discontinuous slope, $E_{m,n_r} \simeq \kappa(n_r)|m|$, when $E_{m,n_r} > 0$.

B. Phases of eigenfunctions

To make later formulas as simple as possible, the phases of the eigenfunctions should be defined so that they have a nontrivial monodromy of their own. To define the phases, we use the following process. For all (m,n_r) we define

$$\psi_{m,n_r}(\rho,\varphi) = N_{m,n_r}\exp(im\varphi)\mathcal{R}_{n_r}^m(\rho), \tag{14}$$

$$\mathcal{R}_{n_r}^m(\rho) = ph(m,n_r)R_{n_r}^{|m|}(\rho). \tag{15}$$

$ph(m,n_r)$ is a phase which is a multivalued function of (m,n_r). It is defined by following paths in quantum spectrum space.

A quantum path in quantum spectrum space is a sequence of discrete steps, with each step connecting a state (m,n_r) to a neighboring state. States (m,n_r) and (m',n_r') are neighbors if $m' = m \pm 1$ or m, and $n_r' = n_r \pm 1$ or n_r. To define the phase, let us take our paths to begin at any fixed n_r, with $m \geqslant 0$. Then at the beginning of a path, we choose $ph(m,n_r) = 1$. If the path crosses the line $m = 0$ at a value of n_r such that $E_{m,n_r} > 0$, the phase becomes

$$ph(-|m|,n_r) = (-)^m ph(|m|,n_r). \tag{16}$$

The same holds if it crosses back to positive m if $E_{m,n_r} > 0$. However, if the path crosses the line $m = 0$ in either direction when $E_{m,n_r} < 0$, then

$$ph(-|m|,n_r) = ph(|m|,n_r). \tag{17}$$

A consequence is that the phase is path dependent. Furthermore, if we follow a closed path in spectrum space that encloses the monodromy center once, then the final phase differs from the initial phase:

$$\mathcal{R}_{n_r}^m(\rho;\text{final}) = (-)^m\mathcal{R}_{n_r}^m(\rho;\text{initial}). \tag{18}$$

After two such circuits, $\mathcal{R}_{n_r}^m(\rho;\text{final}) = \mathcal{R}_{n_r}^m(\rho;\text{initial})$, Eqs. (16) and (17) correspond, respectively, to symmetry relationships of Bessel functions $J_m(\rho)$ or $I_m(\rho)$. (See Fig. 4.)

C. Quantum monodromy circuits

A quantum monodromy circuit is a closed quantum path in quantized spectrum space following quantized smooth action

variables in a circuit around the monodromy center. I_s and $l = m\hbar$ are smooth actions, so n_s and m are quantized smooth action variables. Thus a quantum monodromy circuit is a sequence of steps connecting neighbors as defined above, but with the restriction that we follow quantum numbers associated with smooth action variables. The selected quantum monodromy circuit shown in red in Fig. 3 starts with $m = 0$ and $n_s = n_r = 13$; it goes to $m = 12$ holding n_r at 13, then increases n_r to 28 with m fixed, then decreases m with n_r fixed as long as $m \geqslant 0$. Upon crossing the $m = 0$ axis, since $E > 0$, it follows the smooth action variable $n_s = 28 = \text{const.}$; hence each time m is reduced by 1, n_r is reduced by 1. The upper left corner of the circuit still has $n_s = 28$ but $n_r = 22$, since $m = -6$. The lower left corner has $n_s = 13$; therefore $n_r = 7$. (Here is the multivaluedness of this quantum number; if we had followed a negative-energy path from positive m to this state ($m = -6, n_r = 7$), then its smooth quantum number would be $n_s = 7$ instead of 13). Coming back to $m = 0$, the contours of constant smooth action slope steeply upwards, and we arrive at $m = 0$ with $n_s = 13$, as in the initial state.

D. Superposition states

Here we define a set of nonstationary superposition states which display the topological change similar to that of the action loops as in Fig. 1. That topological change is robust, so there are many ways to choose such superpositions.

Each superposition that we construct has a fixed value of n_s, and a range of m about a central value, called $\hat{m}$. The subscript $[m, n_r(m)]$ means that for each m, there is one and only one value of n_r; it is the value such that n_s is the same in every term. The radial eigenfunctions $\mathcal{R}_{n_r}^m$ are uniquely labeled by quantum numbers n_r and m, except for their phases, which are path dependent. The path used to define the phase $ph(m, n_r)$ is specified as the path to reach $(\hat{m}, n_s)$ together with a few steps in m at fixed n_s. We choose a superposition

$$\psi_{\hat{m}, n_s}(\rho, \varphi) = \sum_m C_{m, n_r(m)}^{\hat{m}, n_s} N_{m, n_r(m)} \mathcal{R}_{n_r(m)}^m(\rho) \exp(im\varphi). \quad (19)$$

The coefficients $C_{m, n_r(m)}^{\hat{m}, n_s}$ are a Gaussian function centered at $\hat{m}$ with a fixed value of n_s:

$$C_{m, n_r(m)}^{\hat{m}, n_s} = \exp\left[-\left(\frac{m - \hat{m}}{2.5}\right)^2\right]. \quad (20)$$

E. Static monodromy in the Mexican hat system

Now we carry this superposition around a monodromy circuit (Figs. 2 and 5). (i) We start with all coefficients zero except for those at one fixed $n_r = n_s^i (= 13)$, and with m having a Gaussian distribution centered at $\hat{m} = 0$, $C_{m, n_r=13}^{0,13} = \exp[-(m/2.5)^2]$. (See Fig. 5.) The value of n_s^i is chosen such that the energy is well below zero. (ii) Holding n_s^i fixed, we increase $\hat{m}$, and keep the Gaussian distribution of coefficients, $\exp[-(m - \hat{m})^2/2.5^2]$. When $\hat{m}$ is sufficiently large, coefficients having $m \leqslant 0$ are negligible, and we set them to zero. (iii) Now at each m, we increase n_s in integer steps until the energy is well above zero. We stop at $n_s = n_r = 28$. At this point the action-angle loop is plainly manifested in the quantum wave function, and it lies on one side of the classically forbidden region [Fig. 2(b)]. (iv) Now we decrease $\hat{m}$, moving
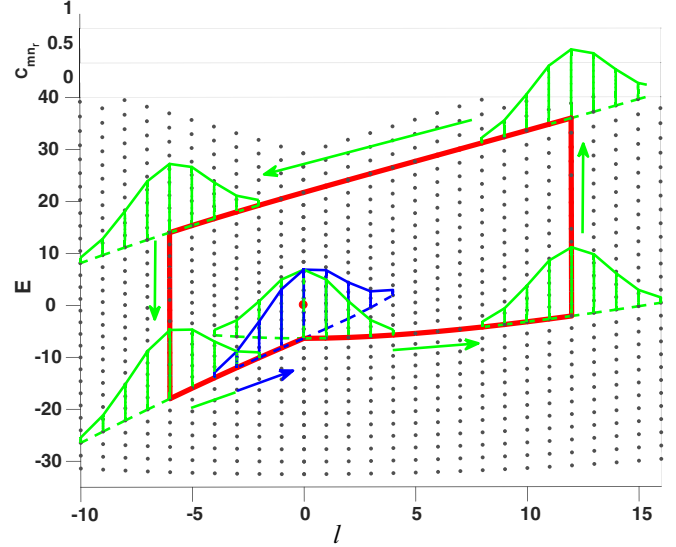

FIG. 5. For the Mexican hat system, a three-dimensional (3D) plot of coefficients $C_{m, n_r}^{\hat{m}, n_s}$ versus l and E. As described in Fig. 3, the gray dots are eigenvalues for the Mexican hat, and the selected monodromy circuit (bold, red online) starts from $(l_i = 0, E_i = E_{m=0, n=13} < 0)$, moves in a counterclockwise direction, and returns to the starting point. Initially, we construct a superposition with $n_r = 13$, centered at $\hat{m} = 0$. All the eigenstates included in this superposition have quantized smooth action $= 12.5$. The coefficients $C_{m, n_r(m)}^{\hat{m}, n_s}$ [Eq. (20)] are represented by the light gray (green online) Gaussian curve centered at (l_i, E_i). Then we take the center of this Gaussian distribution around the monodromy circuit as described in the text. Finally, when we return to the initial point (l_i, E_i), where the coefficients are shown in black (blue online), the eigenstates included in the superposition are different from that in the initial superposition, because the contour of smooth action $= 12.5$ is different from the initial contour.

the Gaussian distribution to smaller m. When the value of m in any term in the superposition becomes negative, we keep the value of $n_s (= 28)$ constant by taking $n_r = n_s + m = n_s - |m|$. Thus we are following a quantum monodromy circuit as defined in Sec. IV C: n_r is adjusted so that the smooth action variable is constant. Also as we follow this path we must adjust the (path-dependent) phase, as specified in Sec. IV B. Now the action-angle loop surrounds the origin, and the wave function does also [Fig. 2(c)]. The upper left corner of this monodromy circuit has $\hat{m} = -6, n_s = 28, n_r = 22$. (v) When $\hat{m}$ is sufficiently negative, then the coefficients for $m \geqslant 0$ are negligible, and we set them to zero. Then we reduce each value of n_s in steps of 1. The superposition now has a range of both n_r and m, and at each step $n_r - m = n_s = \text{const}$. When we have reduced n_s such that that constant equals the initial value of $n_s = n_s^i (= 13)$, we stop reducing n_s. (vi) Finally we increase $\hat{m}$ (the center of the distribution), always keeping n_s constant. This holds also for $m > 0$, and we give attention to the monodromy of the phases. We stop at $\hat{m} = 0$. For the basis functions having $m > 0$, we have crossed the $m = 0$ line below the monodromy center, so we use the symmetry relationship (17). At this final point we have a superposition of eigenfunctions that is different from the original one. For each m, the radial quantum number n_r has changed, and the signs of the basis functions $\mathcal{R}_{n_r}^m$ have changed according to Eqs. (16) and (17).
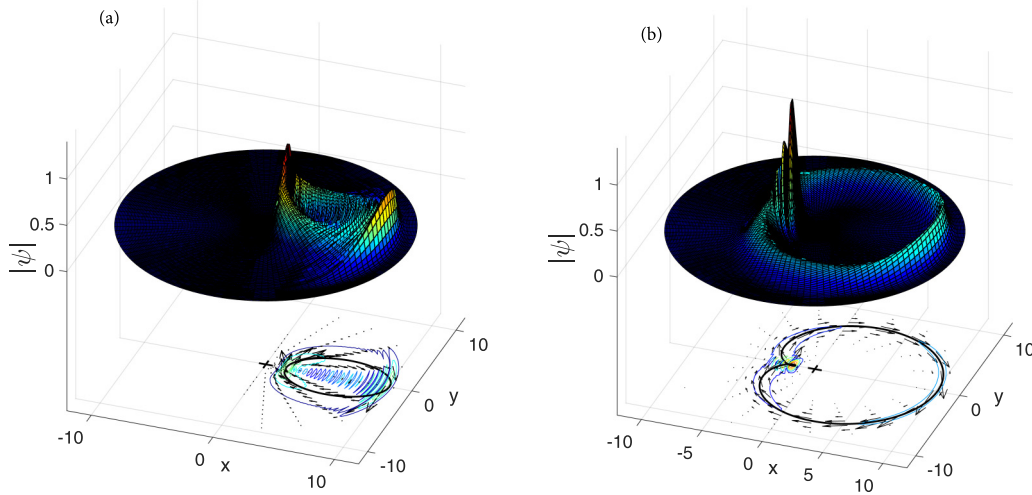
FIG. 6. The surfaces represent the absolute value of wave functions versus Cartesian coordinates (x, y). Below each is the corresponding contour plot, and the probability current (black arrows). The cross markers in the center of the lower planes mark the origin of the (x, y) planes. Those origins are surrounded by classically forbidden regions. The wave function in (a) is described in Eq. (19) with $\hat{m} = 12, n_s = 23$. The one in (b) is the state after once around a monodromy circuit starting from the state in (a). It also has $\hat{m} = 12$, and the central value of $n_s = 23$. It is evident that these wave functions have different winding numbers around the classically forbidden regions. The flux density was computed based on the Hamiltonian $\mathcal{H}$; it is the same as the flux density under the Hamiltonian H as seen in a frame of reference rotating about the origin with angular velocity Ω. These are nonstationary states of the Hamiltonian H; if we include time factors, they rotate about the origin. The bold black loops in the (x, y) planes are classical action-angle loops projected into the plane.

The final superposition surrounds the classically forbidden region [Fig. 2(d)]. *We have obtained static monodromy of superpositions of eigenfunctions.* This is a fully quantum-mechanical monodromy, with little reference to classical or semiclassical mechanics. (We defined n_s to be the quantum number associated with a smooth classical action, but it could have been defined by study of the defect in the spectrum.) If this monodromy process sounds complicated (and perhaps artificial), we emphasize that there are dynamical processes that follow monodromy circuits. A classical process was shown in Ref. [22], and a quantum process will be shown in Sec. VI.

F. Probability current under effective Hamiltonian $\mathcal{H}$

In Fig. 2, we showed that the superposition defined in (19) has the shape of the angle loop. In this section, we show that not only the shape, but also the density flux follows the corresponding angle loop. The probability current or flux density $\vec{j}$ is the flow of probability density such that

$$\frac{d\psi^*\psi}{dt} + \nabla \cdot \vec{j} = 0. \tag{21}$$

Under the effective Hamiltonian (5) which generates the angle loop, we get an unusual form for the flux density:

$$
\begin{aligned}
\frac{d\psi^*\psi}{dt} &= \psi^* \frac{d\psi}{dt} + \frac{d\psi^*}{dt}\psi = \psi^* \frac{1}{i\hbar} H\psi + \psi \frac{1}{-i\hbar} H^\dagger \psi^* \\
&= \nabla \cdot \left[\frac{\hbar}{2\mu i}(\psi\nabla\psi^* - \psi^*\nabla\psi) - \Omega\psi^*\psi(y\vec{i} - x\vec{j}) \right] \\
&= -\nabla \cdot \vec{j}.
\end{aligned}
$$

It follows that the flux density is

$$\vec{j} = \frac{\hbar}{2\mu i}(\psi^*\nabla\psi - \psi\nabla\psi^*) + \Omega\psi^*\psi(y\vec{i} - x\vec{j}). \tag{22}$$

The term containing Ω is unusual but important. If time-dependent phases $\exp(-iE_{m,n}t/\hbar)$ are incorporated, then the wave function rotates about the center. The flux density (22) refers to a frame rotating at the classical rotation rate.

In Fig. 6, two superpositions along with their probability current are plotted. The one labeled (a) is before the monodromy circuit, and the one labeled (b) is after. They have the same expectation values of $\langle l \rangle$ and $\langle E \rangle$. But they have different topological structures and the flux densities have different winding numbers about the origin.

V. INSIGHTS FROM THE CIRCULAR BOX SYSTEM

We arrived at the results given in the preceding section by studying a simpler system, a particle in a circular box. In so doing, we obtained two results of general interest: (1) We show the relationship between the topological changes in the action loops and those in the superposition states using a semiclassical approximation; (2) we show that even for a circular box system, which does not have monodromy, when we examine action loops and wave functions in configuration space, they display topological changes similar to those shown in Figs. 1 and 2.

A. Classical and quantum behavior of the circular box system

Let us consider a circular box with

$$
\begin{aligned}
V(\rho) &= 0, \quad \rho \leqslant \rho_{\max}, \quad V(\rho) = \infty, \quad \rho > \rho_{\max}, \\
\rho_{\max} &= 11.6928.
\end{aligned} \tag{23}
$$

(There is nothing special about this value of $\rho_{\max}$.) We can calculate action-angle loops for this system by integrating trajectories of the effective Hamiltonian, Eq. (5), with this circular box potential, Eq. (23). $\Omega(l, E)$ is, as before, the average angular velocity in a radial cycle of motion, $\Omega(l, E) =$
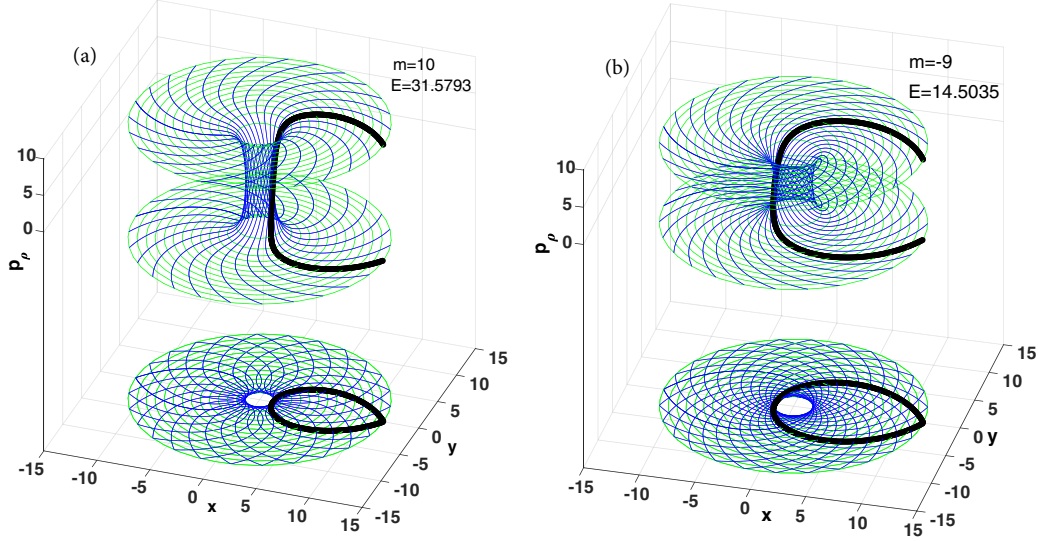
FIG. 7. A topological change of angle variable in the circular box system. This system does not have a complete monodromy circuit, because it does not have negative energies. However, the angle loops have a topological change similar to what occurs on the upper portion of a monodromy circuit in the Mexican hat system. Thus, we compare two tori specified by two points on the incomplete monodromy circuit. (a) The torus in phase space specified by $(l = 10, E = 31.5793)$ and its projection onto the x-y plane. (b) The torus in phase space specified by $(l = -9, E = 14.5035)$ and its projection onto the x-y plane. Due to reflection at the outer hard wall, the "loops" and "tori" jump from positive to negative p_ρ. The coordinate systems, marked by the dark gray (blue online) and light gray (green online) loops, are defined by angle variables (ϕ_1, ϕ_2). The bold black loop is one of the angle loops, defined by $\phi_1 = $ const., $0 < \phi_2 < 2\pi$. In (a), the black angle loop stays on one side of the central forbidden region. When (l, E) change smoothly, the torus changes smoothly, as do the angle loops associated with I_s. When $l < 0$, the angle loop changes into a topologically different loop, shown in (b).

$\frac{\Theta(l,E)}{T(l,E)}$. We must choose $\Theta(l, E)$ to be smooth through $l = 0$, and this can be done if $\Theta(l_{\max}, E) = 0$, $\Theta(l_{\min}, E) = 2\pi$, where $l_{\max}$ and $l_{\min}$ are the maximum and minimum possible values for l at the given energy E. Then

$$T(l, E) = 2\sqrt{\frac{\rho_{\max}^2 - \frac{l^2}{2\mu E}}{2\mu E}},$$

$$\Theta(l, E) = \begin{cases} 2 \arccos\left(\frac{l}{\rho_{\max}\sqrt{2\mu E}}\right), & \text{if } l \geqslant 0 \\ 2\pi - 2\arccos\left(\frac{l}{\rho_{\max}\sqrt{2\mu E}}\right), & \text{if } l < 0 \end{cases}. \quad (24)$$

We show in Fig. 7 trajectories under $\mathcal{H}$ for our selected $l_{\text{initial}} = 10\hbar$ and $E_{\text{initial}} = 31.5793$. This corresponds to the radial quantum number $n_r = 25$, and the value of the smooth action variable $I_s = 24.5\hbar$. We follow a path similar to the top portion of a monodromy circuit by choosing E such that $I_s(l, E)$ is held constant at $24.5\hbar$ while we reduce l continuously until $l_{\text{final}} = -9\hbar$. When l passes through zero, $\Theta(l, E)$ increases smoothly through π. The result is that the action loop defining I_s changes its topological structure relative to the classically forbidden region surrounding the origin: It changes from a loop on one side of the forbidden region to a loop that surrounds that region. As a result, the smooth action variable has the behavior given that in Eq. (8),

$$I_s(-|l|, E) = I_s(|l|, E) - l.$$

As we see in Fig. 7(a), the resulting action loops have the same topological change as was obtained for the Mexican hat potential.

For a quantum particle in a circular box, the radial factors in the eigenfunctions of H and of $\mathcal{H}$ are Bessel functions,

$$\psi_{m,n_r}(\rho, \varphi) = N_{m,n_r} J_m(k_{m,n_r}\rho)\exp(im\varphi), \quad (25)$$

where m is the integer angular momentum quantum number, and $\{k_{m,n_r}\}$ are values such that $J_m(k_{m,n_r}\rho_{\max}) = 0$. The eigenvalues of H are given by

$$E_{m,n_r} = (\hbar k_{m,n_r})^2/2\mu. \quad (26)$$

The quantum number $n_r(=1, 2, ...)$ represents the number of radial nodes in the eigenfunction, including the node at $\rho_{\max}$ but not the node at $\rho = 0$ (when $|m| > 0$). We show in Fig. 8 the grid of eigenvalues (m, E_{m,n_r}). Every eigenfunction of $H(\mathbf{q}, -i\hbar\nabla)$ is also an eigenfunction of $\mathcal{H}(\mathbf{q}, -i\hbar\nabla; l, E)$, but the eigenvalues $\mathcal{E}_{m,n_r}$ of $\mathcal{H}$ are different from those of H:

$$\mathcal{E}_{m,n_r} = E_{m,n_r} - m\hbar\Omega(\ell = m\hbar, E_{m,n_r}). \quad (27)$$

If we use a semiclassical approximation to calculate the eigenvalues, the quantization condition for the radial eigenfunctions is $I_{\text{rad}} = \oint p_\rho d\rho/2\pi = (n_r - \frac{1}{2})\hbar$. States can also be labeled by quantum numbers associated with smooth action variables. If we use $I_s(l, E) = I_{\text{rad}}(l, E)$ for $l \geqslant 0$, then $n_s = n_r$ if $m \geqslant 0$, but $n_s = n_r - m$ for $m < 0$. In this case, quantum states and their energies are uniquely labeled by either (m, n_r) or (m, n_s).

B. Semiclassical approximation

In this section and the next we construct semiclassical wave functions that are localized near a selected
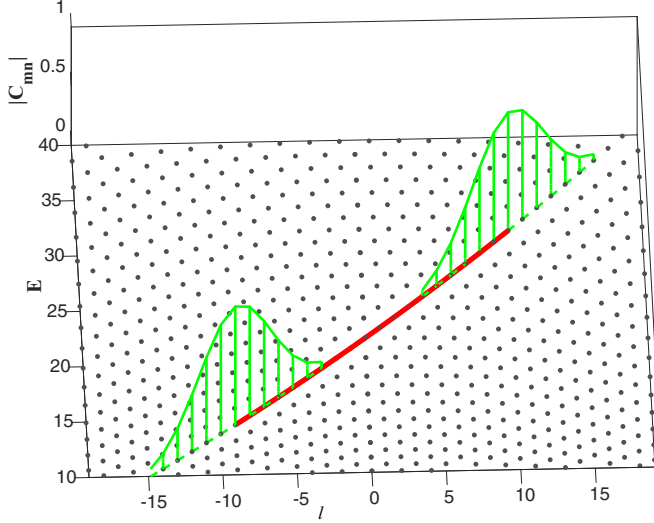
FIG. 8. For the circular box, 3D plot of coefficients versus l and E. As described in Fig. 3, the gray dots are eigenvalues for the circular box. The heavy black (red online) line is a line of constant smooth action, which starts from $(l_i = 10, E_i = E_{\hat{m}=10,\hat{n}_r=25} = 31.5793)$ and links states of quantized smooth action $= 24.5$. The radial quantum number n_r is 25 for $m \geqslant 0$, but $n_s = \hat{n}_r - \hat{m} = 25$ for $m < 0$. The line ends at $l_f = -9, E_f = E_{\hat{m}=-9,\hat{n}_r=16} = 14.5035$. For the initial superposition, the coefficient of each eigenstate ψ_{m,n_r} is plotted as the right-hand light gray (green online) curve: The only nonzero coefficients are those for the eigenstates of quantized smooth action $= 24.5$ and with m between 4 and 16. We find numerically that these coefficients have approximately a Gaussian distribution along the contour of smooth action $=24.5$, centered at (l_i, E_i). Then we push that Gaussian distribution along the black (red online) path, keeping smooth action $=24.5$, until the final point (l_f, E_f), where m ranges from -15 to -3.

action-angle loop. There are two steps. (i) Construct semiclassical approximations to $\psi_{m,n_r}(\rho,\varphi)$. (ii) Construct superpositions that are localized in angle.

A two-dimensional semiclassical approximation to these eigenfunctions of the circular box, $\psi_{m,n_r}(\rho,\varphi)$, can be constructed by the usual rules. However, we use $\mathcal{H}$ as the Hamiltonian instead of H. In this relatively simple system, analytical results can be given.

(a) Specify the quantum numbers $(\hat{m}, n_r)$ of the target eigenfunction. The eigenvalues of angular momentum and energy H are, respectively, $(\hat{m}\hbar, E_{\hat{m},n_r})$. (b) Choose an initial curve in (ρ,φ) space (we take $\rho = \rho_{\max}$), and specify the value of $\psi_{\hat{m},n_r}(\rho,\varphi)$ on that curve. We take it to be $\psi_{\hat{m},n_r}(\rho_{\max},\varphi) = f(\varphi)\exp(i\hat{m}\varphi)$, and temporarily $f(\varphi) = 1$. (c) Define the initial classical momentum on that curve such that

$$p_\varphi = \hat{m}\hbar \tag{28}$$

and

$$\mathcal{H}(\mathbf{q},\mathbf{p}; \hat{m}\hbar, \mathcal{E}_{\hat{m},n_r}) = \mathcal{E}_{\hat{m},n_r}, \tag{29}$$

which is equivalent to

$$H(\mathbf{q},\mathbf{p}) = E_{\hat{m},n_r}. \tag{30}$$

(d) Starting at $\rho_{\max}$, for each initial $\varphi \equiv \varphi_0$, integrate the equations of motion under $\mathcal{H}(\mathbf{q},\mathbf{p})$ to obtain $\mathbf{q}(t,\varphi_0)$, and

$\mathbf{p}(t,\varphi_0)$. The phase of the wave function is constructed by integrating one more equation to obtain the action function $S(t,\varphi_0)$ using

$$\frac{dS}{dt} = \mathbf{p}(t,\varphi_0) \cdot \frac{d\mathbf{q}(t,\varphi_0)}{dt}, \tag{31}$$

with initial condition $S(t = 0,\varphi_0) = m\varphi_0$. In the present case, the trajectories are given by

$$x(\varphi_0,t) = (\rho_{\max} + v_{x0}t)\cos(\Omega t - \varphi_0) + v_{y0}t\sin(\Omega t - \varphi_0), \tag{32}$$

$$y(\varphi_0,t) = -(\rho_{\max} + v_{x0}t)\sin(\Omega t - \varphi_0) + v_{y0}t\cos(\Omega t - \varphi_0), \tag{33}$$

$$p_x(\varphi_0,t) = \mu v_{x0}\cos(\Omega t - \varphi_0) + \mu v_{y0}\sin(\Omega t - \varphi_0), \tag{34}$$

$$p_y(\varphi_0,t) = -\mu v_{x0}\sin(\Omega t - \varphi_0) + \mu v_{y0}\cos(\Omega t - \varphi_0). \tag{35}$$

(e) Invert the relationship $\mathbf{q}(t,\varphi_0)$ [Eqs. (32) and (33)] to obtain $[t(\mathbf{q}),\varphi_0(\mathbf{q})]$ and express the action as a function of $\mathbf{q}$. That inversion gives for each $\mathbf{q}$ two pairs of values $[t(\mathbf{q}),\varphi_0(\mathbf{q})]$, corresponding to the incoming and outgoing waves. (f) The amplitude is found from

$$A(t,\varphi_0) = f(t,\varphi_0)\left|\frac{\mathscr{J}(t = 0,\varphi_0)}{\mathscr{J}(t,\varphi_0)}\right|^{1/2}, \tag{36}$$

which also must be expressed as a function of $\mathbf{q}$. $\mathscr{J}(t,\varphi_0)$ is the Jacobian matrix defined as $\mathscr{J}(t,\varphi_0) \equiv \frac{\partial(x,y)}{\partial(t,\varphi_0)}$.

(g) The semiclassical approximation to $\psi_{m,n}(\rho,\varphi)$ is then

$$\psi_{m,n_r}^{sc}(\rho,\varphi) = A_{in}(\rho,\varphi)\exp\left[\frac{i S_{in}(\rho,\varphi)}{\hbar}\right] + A_{\text{out}}(\rho,\varphi)\exp\left(i\left[\frac{S_{\text{out}}(\rho,\varphi)}{\hbar} - \frac{\pi}{2}\right]\right). \tag{37}$$

In the present case, the amplitude and the phase can be written analytically, and the result is, for the incoming wave,

$$S_{in}(\rho,\varphi) = -|m|\left[\frac{\sqrt{\rho^2 - \rho_{\min}^2}}{\rho_{\min}} - \arccos\left(\frac{\rho_{\min}}{\rho}\right) \right.$$
$$\left. - \frac{\sqrt{\rho_{\max}^2 - \rho_{\min}^2}}{\rho_{\min}} + \arccos\left(\frac{\rho_{\min}}{\rho_{\max}}\right)\right] + m\varphi, \tag{38}$$
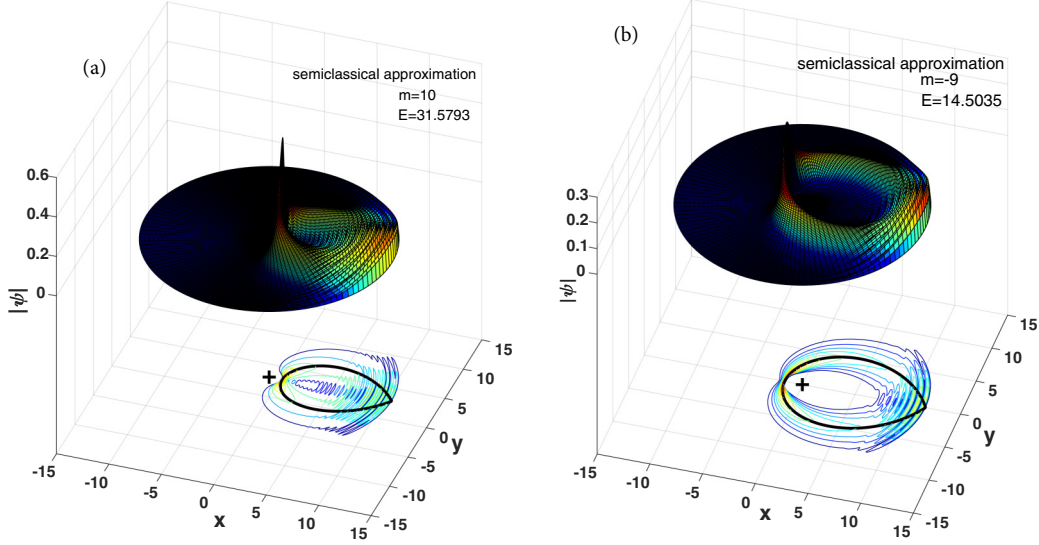
FIG. 9. Topological change of semiclassical wave functions. These two wave functions are localized near the emphasized angle loops on the tori shown in Fig. 7, so they have the same topological change. They were calculated from trajectories having angular momentum and energy (a) $l = 10, E = 31.5793$ and (b) $l = -9, E = 14.5035$, the same as the values in Fig. 7.

while for the outgoing wave,

$$
S_{\text{out}}(\rho,\varphi) = |m| \left[\frac{\sqrt{\rho^2 - \rho_{\min}^2}}{\rho_{\min}} - \arccos\left(\frac{\rho_{\min}}{\rho}\right) \right.
$$

$$
\left. + \frac{\sqrt{\rho_{\max}^2 - \rho_{\min}^2}}{\rho_{\min}} - \arccos\left(\frac{\rho_{\min}}{\rho_{\max}}\right) \right] + m\varphi,
$$
(39)

$$
A_{in}(\rho,\varphi) = A_{out}(\rho,\varphi) = \sqrt{\frac{1}{2\sqrt{\rho_{\max}^2 - \rho_{\min}^2}\sqrt{\rho^2 - \rho_{\min}^2}}},
$$
(40)

where $\rho_{\min} = |l|/\sqrt{p x^2 + p y^2}$.

C. Initial condition localized in φ

We now want to construct wave functions that are not eigenfunctions of H or of H, but instead are localized near one action-angle loop. For this purpose we take $f(\varphi_0) = \exp(-\varphi_0^2/\beta^2)$. This weighting factor makes only one action-angle loop and its neighbors play an important role in the construction of semiclassical wave function. Just as above, for each (ρ,φ), we must find (t,φ_0), and that value of φ_0 is used in $f(\varphi_0)$. Since the resulting function is localized in φ, it no longer has a definite value of angular momentum quantum number $\hat{m}$, and if $\hat{m} <$ or ≈ 0, it no longer has a unique value of n_r. Accordingly, we now label the wave functions and energies by $(\hat{m}, \hat{n}_s)$, $\Psi_{\hat{m}, \hat{n}_s}^{sc}$.

Two such wave functions are shown in Fig. 9. One has $\hat{m} = 10$ and $\hat{n}_r = 25, n_s = 25$ for which $E_{\hat{m}, n_s} = 31.5793$. The other has $\hat{m} = -9\hbar$, $n_s = 25$, and $\hat{n}_r = 25 + (-9)$, for which $E_{\hat{m}, n_s} = 14.5035$. These two wave functions display the

topological change that corresponds to the topological change in the action-angle loops.

D. Repair of divergence

Like all semiclassical approximations, these wave functions diverge at caustics, which in our case are radial turning points, where $A(\rho,\varphi) \to \infty$. We can repair the divergences by expanding $\psi_{\hat{m}, n_s}^{sc}(\rho,\varphi)$ in a small set of eigenfunctions of H:

$$
\psi_{\hat{m}, \hat{n}_s}^{sc}(\rho,\varphi) = \sum_{m,n_r} C_{m,n_r}^{\hat{m}, \hat{n}_s} N_{m,n_r} J_{n_r}^m(\rho) \exp(im\varphi).
$$
(41)

Evaluation of coefficients shows that the expansion is dominated by a small number of terms. If $\hat{m}$ is substantially greater than zero, then only terms of fixed $n_r = n_s (=25)$ have large coefficients, and computation shows that those coefficients are distributed in m approximately as a Gaussian function (Fig. 8). On the other hand, if $\hat{m}$ is substantially less than zero, then the only large coefficients have $n_r - m = n_s$, and the distribution in m is again approximately Gaussian (Fig. 8). Two such superpositions of eigenfunctions are shown together in Fig. 10 with the corresponding semiclassical approximations in Fig. 9. The divergences have been repaired, and the topological change remains.

These superpositions are nonstationary states. If we incorporate the phase factors associated with H, $\exp(-i E_{\hat{m}, n_s} t/\hbar)$, these wave functions revolve around the origin at a rate close to $\Omega(\hat{m}\hbar, E_{\hat{m}, n_s})$.

As stated above, although the circular box does not have monodromy, when we focus on configuration space, action-angle loops and corresponding wave functions have the topological change that was seen in the Mexican hat system. This calculation also provides the motivation for the superpositions that we used in the Mexican hat system [Fig. 5 and Eq. (20)].
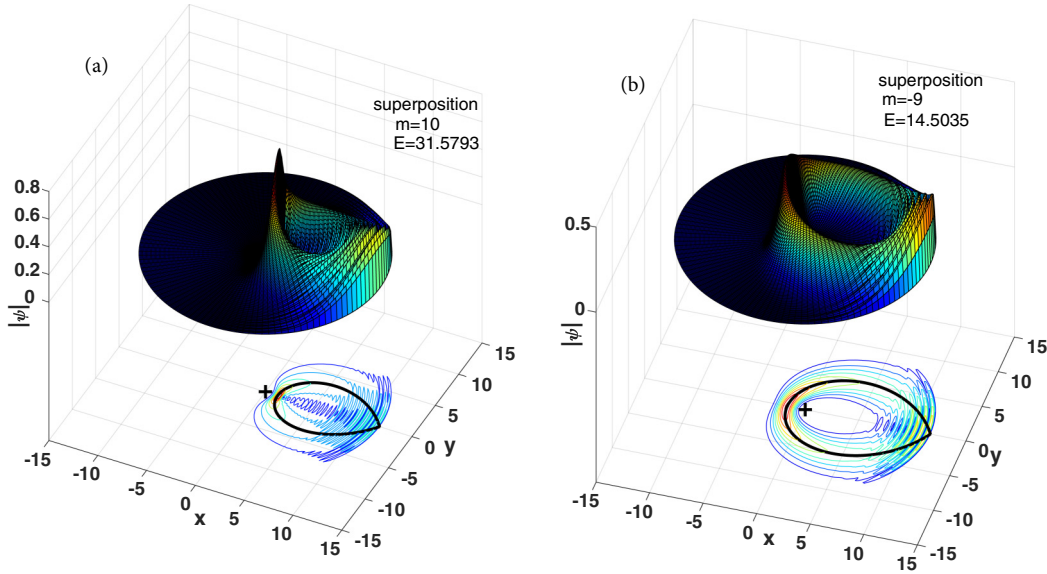
FIG. 10. The wave function in (a) is a superposition of eigenstates of the circular box and has expectation value of angular momentum and energy $\langle l \rangle = 10\hbar, \langle E \rangle \simeq 31.58$. The wave function is large near the corresponding action-angle loop, on one side of the origin. The function in (b) is a superposition with expectation value of angular momentum and energy $\langle l \rangle = -9, \langle E \rangle \simeq 14.50$. It is large near the topologically changed action-angle loop, which surrounds the origin.

VI. DYNAMICAL MANIFESTATION OF MONODROMY

A. Dynamical monodromy of wave functions: ideal evolution

We may define ideal evolution leading to dynamical monodromy of superpositions of eigenfunctions by (1) making the coefficients in the superposition (19) or (41) time dependent, then (2) creating a unitary matrix that continuously changes the coefficients $C_{m,n_r}^{\hat{m},n_s}$ such that they are given by a Gaussian function that continuously follows the monodromy circuit, as in Fig. 5. On the steps with changing angular momentum, we fix n_s and move the center value $\hat{m}$. The coefficients $C_{m,n_r}^{\hat{m},n_s}$ of $\psi_{\hat{m},n_s}$ are

$$C_{m,n_r}^{\hat{m},n_s}(t) \propto \exp\left(-\left[\frac{m - \hat{m}(t)}{2.5}\right]^2\right). \qquad (42)$$

$\hat{m}(t)$ goes continuously from 0 to 12 on the first step, 12 to –6 on the third, and –6 back to zero on the fifth and last step.

On each energy-changing step, the basis functions included in the superposition are from n_s to $n_s \pm 1$. When energy is increasing, we switch the coefficients continuously between n_s and $n_s + 1$ as indicated in Fig. 11, using the formulas

$$\psi(\rho,\varphi;t) = \sum_m w_{n_s}(t) C_{m,n_r(m)}^{\hat{m},n_s}(t) \psi_{m,n_r}(\rho,\varphi) \exp\left(-i E_{m,n_r} t\right)$$

$$+ \sum_m w_{n_s+1}(t) C_{m,n_r(m)}^{\hat{m},n_s+1}(t) \psi_{m,n_r+1}(\rho,\varphi)$$

$$\times \exp(-i E_{m,n_{r+1}} t)\left(\frac{n_s - 3}{5} \leqslant t \leqslant \frac{n_s - 2}{5}\right),$$

$$w_{n_s}(t) = \cos\left[\frac{5}{2}\pi\left(t - \frac{n_s - 3}{5}\right)\right],$$

$$w_{n_s+1}(t) = \sin\left[\frac{5}{2}\pi\left(t - \frac{n_s - 3}{5}\right)\right]. \qquad (43)$$

Similarly on energy-decreasing steps, we go from n_s to $n_s - 1$. The complete wave function on the energy-changing steps is a linear combination of sums over m for n_s and for $n_s \pm 1$. The time-dependent weight for each n_s is shown in Fig. 11 along with the time dependence of $\hat{m}(t)$.

This process produces a kind of ideal evolution, in which the wave function changes its topological structure as in Fig. 2. This ideal quantum evolution is analogous to the ideal classical evolution described in Ref. [21]. (Ideal classical evolution of a family of particles was defined so that all particles evolve continuously and simultaneously from one torus to another.)

B. Dynamical monodromy of wave functions: physical evolution

Finally, let us go back to the circular box, and show that the topological change in the wave function that we saw above can be produced by physical evolution under a time-dependent Hamiltonian. This is analogous to our work in Ref. [22], where we showed that classical evolution under a time-dependent Hamiltonian gives the topological change in a loop of classical particles.

Since for the circular box, the energy cannot be negative, a complete monodromy circuit does not exist. However, we may drive the expectation values of angular momentum and energy along paths of constant smooth action, like the one in Fig. 8. A time-dependent Hamiltonian which accomplishes that is

$$H(t) = H_0(\boldsymbol{q}, -i\hbar\nabla) + P(\boldsymbol{q}, t), \qquad (44)$$

where $H_0(\boldsymbol{q}, -i\hbar\nabla)$ is exactly the Hamiltonian in Eq. (1), with the circular box potential. $P(\boldsymbol{q}, t)$ is a perturbation produced by a counterclockwise rotating uniform force $|\mathbf{F}| = 0.05$ with a direction and rotation rate designed to decrease the expectation value of angular momentum $\bar{l}$. For those who may wish to reproduce our results, the azimuthal angle defining the
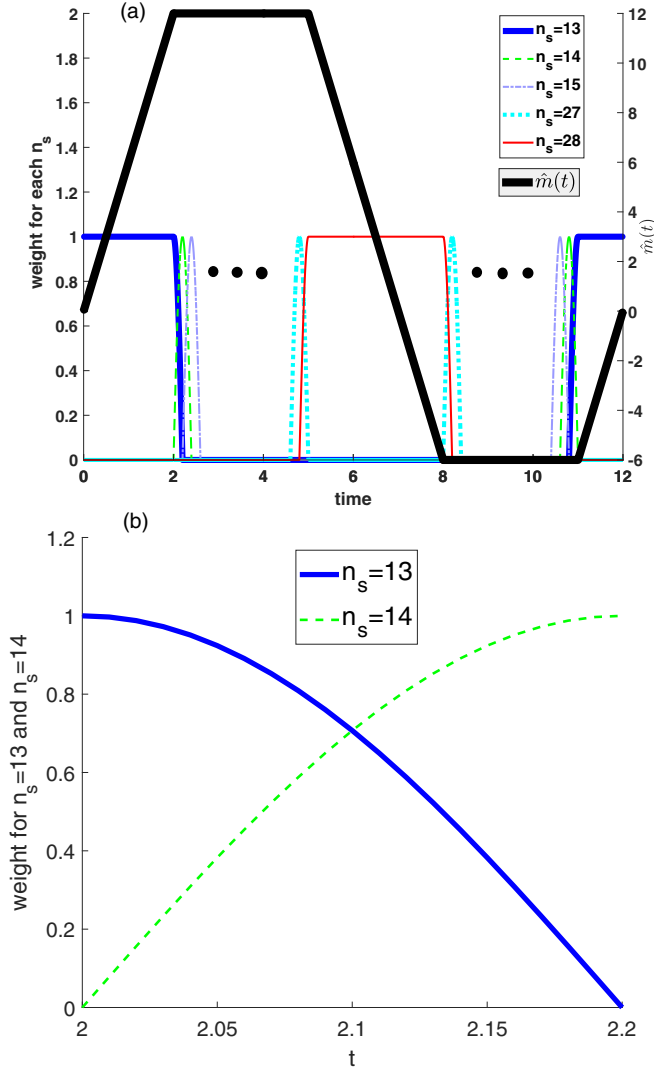
FIG. 11. The unitary transformation. (a) The heaviest black line, varying from 0 to 12 to -6 and back to 0, shows how the center angular momentum number $\hat{m}(t)$ changes with time during the transformation. Each of the other (colored online) curves represents a weighting factor $w_{n_s}(t)$. Two weighting factors for $n_s = 13$ and $n_s = 14$ are magnified in (b). The $w_{13}(t)$ begins equal to 1, and at $t = 2$, it begins to decrease, reaching zero at $t = 2.2$, where $w_{14}(t)$ has increased to 1. Subsequently, each $w_{n_s}(t)$ for n_s between 15 and 28 rises and falls. The sequence is represented by the ellipses $(\cdots)$ in the figure.

direction of the force was taken to be

$$\varphi(t) = \frac{105.1t^2 + 406.6t - 36.2}{t^2 + 219t - 19.14}. \tag{45}$$

The initial superposition is similar to that shown in Fig. 10, but with a lower energy. Coefficients are nonzero only for $n_s = n_r = 10$; the coefficient distribution is Gaussian, centered at $\hat{m} = 10$:

$$C_{m,10} = \exp\left[-\left(\frac{m - \hat{m}}{2.5} \right)^2 \right]. \tag{46}$$

With the time-dependent Hamiltonian (44), we solve the Schrödinger equation in a basis set including m from -9 to 15 and n_r from 1 to 13. Remarkably, it turns out that the dominant

coefficients are always those with $n_s = 10$ (i.e., when $m \geqslant 0$, $n_r = 10$ or when $m < 0$, $n_r - m = 10$). Furthermore, the distribution in m remains approximately Gaussian, with

$$|C|_{m,n_r} \simeq \exp\left(-\left[\frac{m - \hat{m}(t)}{2.5} \right]^2 \right). \tag{47}$$

As the expectation value of $\hat{m}$ decreases, the expectation value of E also decreases so that the path traced out by $(\hat{m}\hbar, E)$ is similar to the path shown in Fig. 8. Those paths have constant values of the smooth action variable $I_s(l, E)$. They are in effect the upper portion of a monodromy circuit. Thus we have shown that this simplest of all possible quantum dynamical processes follows the states associated with the smooth action variable.

Two movies are included in the Supplemental Material [55]. One shows the topological change of the time-dependent wave function and the other shows absolute values of the coefficients C_{m,n_r}, changing with time.

It is pleasing to see that the mode of the wave function $|\psi(\mathbf{q},t)|$ shows the desired topological change during this process. Thus we have shown that the topological change in wave functions can be made to occur using an ordinary Hamiltonian with a rotating force.

VII. CONCLUSION

As stated in the abstract, and displayed in Sec. I, we have shown that simple two-dimensional systems can show topological changes in wave functions, changes that are analogous to the topological changes in action-angle loops. The shape of the superposition and the probability current follow the shape and current of the corresponding action-angle loop.

In Sec. III, we introduced single-valued radial action variables $I_{\rm rad}$ and multivalued smooth action variables I_s, and their corresponding quantum numbers n_r and n_s. Because smooth action variables are multivalued, their corresponding quantum numbers are multivalued (there is no unique assignment of a smooth quantum number to each quantum state). In Sec. IV, we defined a superposition of eigenfunctions of the Mexican hat system, and showed that when this superposition is carried around a monodromy circuit, a topological change in the structure of the wave function is found. To define the superposition, careful attention to the phase of the basis function is required; we define those phases so that they have a monodromy of their own. The topological change in the wave function is robust, and will occur with many different superpositions; we presented a simple case in which the coefficients $C_{m,n_r}^{\hat{m},n_s}$ involve a single smooth action quantum number and a Gaussian distribution in m (Fig. 5). Section V shows how we arrived at these results by study of the simpler circular box system.

Section VI shows time-dependent dynamical processes leading to the topological change. One is an ideal unitary transformation, in which time-dependent coefficients for the superposition are defined such that they carry the expectation values of angular momentum and energy around the monodromy circuit. The other is evolution under a time-dependent Hamiltonian having a rotating force. This evolution shows that, just as classical dynamical processes may follow the behavior of smooth action and angle variables, producing a topolog-

ical change in a loop of particles [22], quantum dynamical processes may follow the quantum states corresponding to smooth-action variables, and produce a topological change in a quantum wave function.

[1] R. Cushman and D. Sadovskii, Phys. D (Amsterdam, Neth.) **142**, 166 (2000).

[2] R. H. Cushman, H. R. Dullin, A. Giacobbe, D. Holm, M. Joyeux, P. Lynch, D. Sadovskii, and B. Zhilinskii, Phys. Rev. Lett. **93**, 024302 (2004).

[3] M. Sanrey, M. Joyeux, and D. A. Sadovskii, J. Chem. Phys. **124**, 074318 (2006).

[4] A. Giacobbe, R. Cushman, D. Sadovskii, and B. Zhilinskii, J. Math. Phys. **45**, 5076 (2004).

[5] M. Joyeux, D. Sadovskii, and J. Tennyson, Chem. Phys. Lett. **382**, 439 (2003).

[6] B. P. Winnewisser, M. Winnewisser, I. R. Medvedev, M. Behnke, F. C. De Lucia, S. C. Ross, and J. Koput, Phys. Rev. Lett. **95**, 243002 (2005).

[7] M. Winnewisser, B. P. Winnewisser, I. R. Medvedev, F. C. De Lucia, S. C. Ross, and L. M. Bates, J. Mol. Struct. **798**, 1 (2006).

[8] C. A. Arango, W. W. Kennerly, and G. S. Ezra, Chem. Phys. Lett. **392**, 486 (2004).

[9] C. R. Schleif and J. B. Delos, Phys. Rev. A **76**, 013404 (2007).

[10] C. R. Schleif and J. B. Delos, Phys. Rev. A **77**, 043422 (2008).

[11] N. J. Fitch, C. A. Weidner, L. P. Parazzoli, H. R. Dullin, and H. J. Lewandowski, Phys. Rev. Lett. **103**, 034301 (2009).

[12] D. A. Sadovskii and B. I. Zhilinskii, Mol. Phys. **104**, 2595 (2006).

[13] M. Child, T. Weston, and J. Tennyson, Mol. Phys. **96**, 371 (1999).

[14] M. S. Child, Adv. Chem. Phys. **136**, 39 (2008).

[15] W. Majewski, A. McKellar, D. Sadovskii, and J. Watson, Can. J. Phys. **72**, 1016 (1994).

[16] D. Fontanari and D. A. Sadovskií, J. Phys. A: Math. Theor. **48**, 095203 (2015).

[17] L. Grondin, D. A. Sadovskii, and B. I. Zhilinskii, Phys. Rev. A **65**, 012105 (2001).

[18] H. R. D. Holger Waalkens, Ann. Phys. **295**, 81 (2002).

[19] V. I. Arnold, *Mathematical Methods of Classical Mechanics* (Springer, Berlin, 1978).

[20] J. B. Delos, C. R. Schleif, and G. Dhont, J. Phys.: Conf. Ser. **99**, 012005 (2008).

[21] J. Delos, G. Dhont, D. Sadovskii, and B. Zhilinskii, Ann. Phys. **324**, 1953 (2009).

[22] C. Chen, M. Ivory, S. Aubin, and J. B. Delos, Phys. Rev. E **89**, 012919 (2014).

[23] I. C. Percival, J. Phys. B **6**, L229 (1973).

[24] I. Percival, in *Nonlinear Dynamics Aspects of Particle Accelerators*, Lecture Notes in Physics, Vol. 247 (Springer, Berlin, Heidelberg, 1986), pp. 12–36.

[25] M. Berry, J. Phys. A: Math. Gen. **10**, 2083 (1977).

[26] M. V. Berry and M. Tabor, Proc. R. Soc. London, Ser. A **356**, 375 (1977).

[27] D. W. Noid and R. A. Marcus, J. Chem. Phys. **62**, 2119 (1975).

[28] D. W. Noid, M. L. Koszykowski, and R. A. Marcus, Annu. Rev. Phys. Chem. **32**, 267 (1981).

[29] S. K. Knudson, J. B. Delos, and D. W. Noid, J. Chem. Phys. **84**, 6886 (1986).

[30] A. M. O. De Almeida, *Hamiltonian Systems: Chaos and Quantization* (Cambridge University Press, Cambridge, 1990).

[31] M. T. Lopez-Arias, V. R. Manfredi, and L. Salasnich, Riv. Nuovo Cimento **17**, 1 (1994).

[32] J. J. Duistermaat, Commun. Pure Appl. Math. **33**, 687 (1980).

[33] R. Cushman and J. J. Duistermaat, Bull. Am. Math. Soc. **19**, 475 (1988).

[34] B. Zhilinskií, Acta Appl. Math. **87**, 281 (2005).

[35] N. N. Nekhoroshev, D. A. Sadovskií, and B. I. Zhilinskií, Ann. Henri Poincare **7**, 1099 (2006).

[36] N. N. Nekhoroshev, D. A. Sadovskií, and B. I. Zhilinskií, C. R. Math. **335**, 985 (2002).

[37] K. Efstathiou, R. Cushman, and D. Sadovskii, Adv. Math. **209**, 241 (2007).

[38] M. Hansen, F. Faure, and B. Zhilinskií, J. Phys. A: Math. Theor. **40**, 13075 (2007).

[39] D. Sugny, A. Picozzi, S. Lagrange, and H. R. Jauslin, Phys. Rev. Lett. **103**, 034102 (2009).

[40] R. H. Cushman and L. M. Bates, *Global Aspects of Classical Integrable Systems* (Birkhäuser, Basel, 1997).

[41] K. Efstathiou and D. Sadovskií, Rev. Mod. Phys. **82**, 2099 (2010).

[42] D. J. Thouless, M. Kohmoto, M. P. Nightingale, and M. den Nijs, Phys. Rev. Lett. **49**, 405 (1982).

[43] Q. Niu, D. J. Thouless, and Y.-S. Wu, Phys. Rev. B **31**, 3372 (1985).

[44] D. J. Thouless, Phys. Rev. B **27**, 6083 (1983).

[45] S. Nakajima, T. Tomita, S. Taie, T. Ichinose, H. Ozawa, L. Wang, M. Troyer, and Y. Takahashi, Nat. Phys. **12**, 296 (2016).

[46] M. Lohse, C. Schweizer, O. Zilberberg, M. Aidelsburger, and I. Bloch, Nat. Phys. **12**, 350 (2015).

[47] A. Y. Kitaev, Ann. Phys. **303**, 2 (2003).

[48] S. D. Sarma, M. Freedman, and C. Nayak, Phys. Today **59**, 32 (2006).

[49] M. Freedman, A. Kitaev, M. Larsen, and Z. Wang, Bull. Am. Math. Soc. **40**, 31 (2003).

[50] J. K. Pachos, *Introduction to Topological Quantum Computation* (Cambridge University Press, Cambridge, 2012).

[51] J. Pachos, Phys. Rev. A **66**, 042318 (2002).

[52] J. Pachos and S. Chountasis, Phys. Rev. A **62**, 052318 (2000).

[53] J. K. Pachos and S. H. Simon, New J. Phys. **16**, 065003 (2014).

[54] E. Dennis, A. Kitaev, A. Landahl, and J. Preskill, J. Math. Phys. **43**, 4452 (2002).

[55] See Supplemental Material at http://link.aps.org/supplemental/10.1103/PhysRevE.97.062216 for figures with two families of action-angle loops, and two movies about time-dependent evolution of a wave packet.